

Article

# Research on a Variable-Stiffness Joint and Its Application in Actuators

Qi Wang <sup>1,\*</sup>, Xiaolong Lu <sup>1</sup>, Peng Jiang <sup>1</sup>, Chang Guo <sup>1,\*</sup>  and Yalin Sun <sup>2</sup>

<sup>1</sup> School of Mechanical Engineering and Rail Transit, Changzhou University, Changzhou 213164, China; xllu@cczu.edu.cn (X.L.); peng.jiang@cczu.edu.cn (P.J.)

<sup>2</sup> CCZU-ARK Institute of Carbon Materials, Nanjing 210012, China; sunyl@ciomp.ac.cn

\* Correspondence: wangqi0309@126.com (Q.W.); cguo@cczu.edu.cn (C.G.)

**Abstract:** Variable-stiffness actuators can flexibly adjust the overall or local stiffness of a structure, thus enabling reconstruction, adaptation, and locking capabilities that can meet a wide range of task requirements. However, the programmable design and manufacture of three-dimensional (3D) variable-stiffness actuators has become a challenge. In this paper, we present a method to develop the 3D structure of variable-stiffness actuators that combines variable-stiffness joints with 3D printing technology. The variable-stiffness joints were obtained by arranging steel needles wrapped with enameled copper wire inside the grooves of a polylactic acid (PLA) structure and bonding the three components with silicone glue. First, a variable-stiffness joint was used as a variable-stiffness node and subjected to 3D printing to realize multiple 3D variable-stiffness designs and manufacture a programmable structure. Then, using the repulsive force between paired magnets, we developed a driving actuator for the 3D variable-stiffness structure, enabling the expansion and deployment functions of the structure. In addition, an electromagnetically driven mechanical gripper was designed based on variable-stiffness joints to effectively decrease the driving energy in applications where objects are held for extended periods using variable-stiffness control. Our study provides practical solutions and guidance for the development of 3D variable-stiffness actuators, contributing to the achievement of more innovative and practical actuators.

**Keywords:** variable-stiffness joint; variable-stiffness actuator; PLA; self-deforming; 3D printing



**Citation:** Wang, Q.; Lu, X.; Jiang, P.; Guo, C.; Sun, Y. Research on a Variable-Stiffness Joint and Its Application in Actuators. *Actuators* **2023**, *12*, 397. <https://doi.org/10.3390/act12110397>

Academic Editor: Rocco Antonio Romeo

Received: 20 September 2023

Revised: 22 October 2023

Accepted: 24 October 2023

Published: 25 October 2023



**Copyright:** © 2023 by the authors. Licensee MDPI, Basel, Switzerland. This article is an open access article distributed under the terms and conditions of the Creative Commons Attribution (CC BY) license (<https://creativecommons.org/licenses/by/4.0/>).

## 1. Introduction

Variable-stiffness actuators can flexibly adjust the overall or local stiffness of a structure [1–4], thus enabling reconstruction, adaptation, and locking capabilities that can meet a wide range of task requirements [5–7]. For example, combined driver units expand and deploy structures that can be applied in space exploration and in the medical field [8,9]. Variable-stiffness structures have good shape adaptability in the softened state and good load-bearing capacity in the hardened state, which makes them valuable in robotics, as mechanical grippers, and in rehabilitation medicine [7,10–13]. In addition, while soft actuators based on electromagnetic drives and dielectric elastomer drives must continuously provide driving energy when clamping objects, variable-stiffness actuators can clamp objects in a hardened state, which effectively reduces the energy consumption [1,14,15]. Variable-stiffness actuators have been extensively researched in studies on variable-stiffness structures [5,11,15–19]. These studies are primarily based on shape memory polymers [1,16,20] liquid metals [4,15], and particle blocking [19,21] to control the stiffness of the joints or the overall structure of manipulators and improve their bearing capacity, deformation control, and adaptability. However, these studies mainly focused on the deformation modes of bending and torsion. In comparison, 3D variable-stiffness actuators with more deformable variable-stiffness joints have a higher potential for application in various fields.

In recent years, research has been extensively conducted on complex actuators with variable stiffness [6,10,22–24]. For example, a low-temperature liquid metal was injected

into a flexible silicone tube, and an enameled wire was wrapped around it to obtain one-dimensional variable-stiffness fibers. Subsequently, a permanent magnet was attached to it, which could control the shape using an external magnetic field, obtaining an actuator with significant application value in the medical field [22,24]. In addition, researchers have integrated driving components into two-dimensional variable-stiffness structures, using the infinite curvature of the two-dimensional plane to produce complex variable-stiffness actuators [10,23]. These two-dimensional variable-stiffness actuators have potential applications in multimodal vehicles, morphing drones, amphibious robots, reconfigurable exoskeletons, and wearable devices [6,12,25]. However, these variable-stiffness structures cannot be transformed into arbitrary three-dimensional structures because of the continuity of one- and two-dimensional structures, which significantly limits their applications.

Poly(lactic acid) (PLA) is a commonly used consumable for melt deposition 3D printing, which can achieve the rapid prototyping of any complex structure [26,27]. In addition, when PLA temperature exceeds 80 °C (glass transition temperature), shape reshaping can be carried out, which is often used for variable-stiffness actuators [2,8]. For example, segments of heating elements can be arranged on a long PLA strip to create a finger-like variable-stiffness actuator using a shape memory alloy or pneumatic structures [5,14]. Researchers also embedded NiTi wires as heating elements in hollow PLA fibers and wrapped shape memory alloys around the PLA fibers as driving elements to create one-dimensional variable-stiffness actuators [28]. In addition, by combining PLA with materials such as graphene or carbon nanotubes, which possess resistive thermal effects, the stiffness of the PLA structure can be regulated [29,30]. Further, by combining them with driving elements such as magnets or shape memory alloys, variable-stiffness actuators can be obtained [29,30]. However, the above research did not effectively solve the local stiffness control problem in 3D variable-stiffness PLA structures. This would require smaller heating elements that can be conveniently and quickly arranged on the PLA structure. Using thinner enameled copper wires wound around steel needles as heating components can achieve higher heating efficiency in smaller structures, with the steel needles also serving as a support to better position the heating assembly in the 3D PLA structure. Therefore, combining a 3D PLA structure with enameled copper wire/steel needles as heating components has the potential to achieve local stiffness control in three-dimensional structures and further advance the development of 3D variable-stiffness actuators.

This study proposes a method to develop 3D programmable variable-stiffness actuators based on variable-stiffness joints. First, we designed a variable-stiffness joint consisting of steel needles wrapped with enameled copper wire arranged in the grooves of a poly(lactic acid) (PLA) matrix structure and bonded with silicone glue to form the joint. Stiffness control was achieved by applying a current to the enameled copper wire to induce a phase transition in the PLA groove. We then combined the variable-stiffness joints as structural units using the three-dimensional (3D) printing technology to develop two self-deforming variable-stiffness actuators that utilized the repulsive force between paired magnets, achieving the expansion and deployment functions of the structure. Furthermore, we designed an electromagnetically driven mechanical gripper based on the designed variable-stiffness joints, which was shown to effectively decrease the driving energy in applications where objects are held for an extended period using variable-stiffness control.

## 2. Design, Fabrication, and Test of Variable-Stiffness Joints

### 2.1. Materials and Equipment

PLA were purchased from Zhejiang Cixi Lanbo Printing Consumables Co., Ltd. The enameled copper wire's diameter was 1.75 mm, the printing temperature was 190–220 °C, and the bending modulus was 3.3 GPa. Silicone glue (V-1510) was purchased from Guangdong LeLai Adhesive Co., Ltd. and could be used within the temperature range of –50–250 °C. Ecoflex-00-50 was purchased from America Smooth-On, Inc. A magnet (N40UH-NdFeB) was purchased from Jiangsu Suzhou Jinci Magnetic Industry Co., Ltd. A fused deposition modeling (FDM) 3D printer (ZD-210) was purchased from Guangdong

Shenzhen Zhandong Industrial Co., Ltd. A programmable direct-current (DC) power supply (TH6402B) was purchased from Jiangsu Changzhou Tonghui Electronic Co., Ltd. USB 8AD Bipolar data acquisition cards were obtained from Hubei Wuhan YAV Electronics Technology Co., Ltd., and the infrared thermal imager Ui3293 was obtained from Guangdong UniTrend Technology Co., Ltd.

## 2.2. Design and Fabrication

Firstly, we used PLA as a variable-stiffness structure. When heated above 80 °C (glass transition temperature), its stiffness decreases significantly, allowing it to undergo shape remodeling. Secondly, to control the local stiffness of the PLA structure, we used thin steel needles wrapped with enameled copper wire as heating components. By winding the enameled copper wire around the needles, we could effectively improve the heating efficiency while maintaining the size of the heating components small. To integrate the heating components in PLA quickly and firmly, we used a silicone glue as a bonding material between the components.

Based on the above principles, we designed a variable-stiffness joint consisting of a PLA structure, a steel needle, an enameled copper wire, and silicone glue, as shown in Figure 1. The PLA structure was constructed using FDM 3D printing. The diameters of the enameled copper wire and steel needle were 0.15 and 0.5 mm, respectively. The length of the steel needle was 7.5 mm, and the enameled copper wire was wound around the steel needle in 50 turns. This length was approximately equal to the width of the joint, which was 8 mm. We arranged the steel needles wrapped with the enameled copper wire in the grooves of the PLA structure and applied the silicone glue to bond them and form a joint. The enameled copper wire induced a phase transformation in the groove of the PLA structure after electrification and heat generation, achieving stiffness control. The steel needles served as the rotation axis to prevent torsional deformation after joint softening.

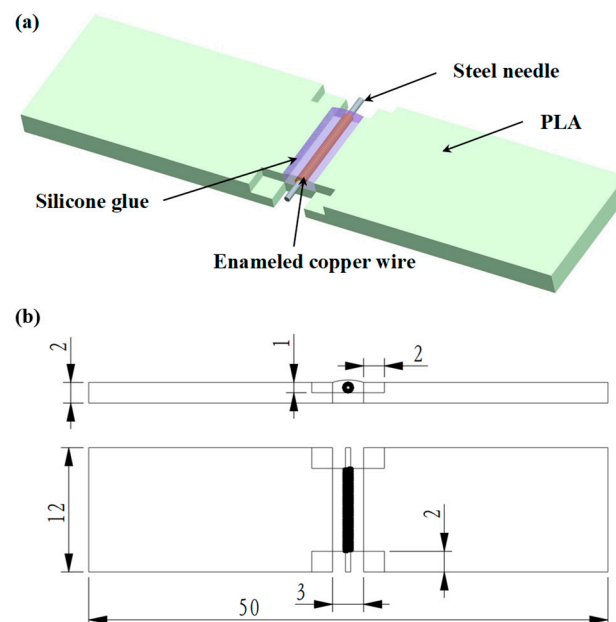


**Figure 1.** Variable-stiffness joint. (a) Diagram of the structure; (b) detailed dimensions.

## 2.3. Heating Curves and Bending Modulus

A programmable DC power supply was used to apply DC current to the enameled copper wire, as shown in Figure 2. Simultaneously, an electric moving stage was used to produce a fixture, which caused the variable-stiffness joint to undergo a bending deformation. The force required to bend the variable-stiffness joint was measured using a force sensor, the heating curves were obtained using a K-type thermocouple temperature sensor, and the data were collected using a data acquisition card. During the test, the fixture

moved at a speed of 50 mm/min. The bending modulus was calculated using the formula  $E = FL^3/3I\delta$ , where  $F$  is the force required by the sample to produce a bending deformation,  $L$  is the length of the sample,  $\delta$  is the displacement (deflection), and  $I$  is the cross-sectional moment of inertia of the sample.

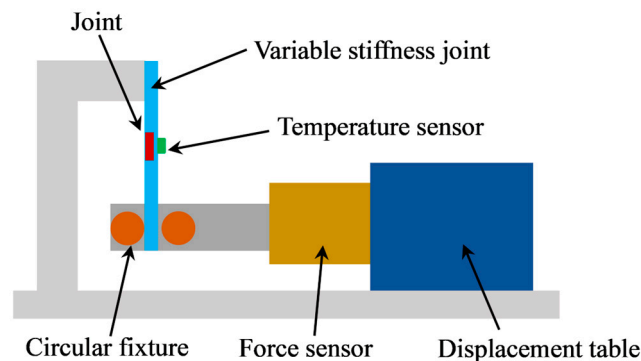


**Figure 2.** Schematic diagram of the testing device to obtain heating curves and bending modulus.

#### 2.4. Cyclic Deformation Ability

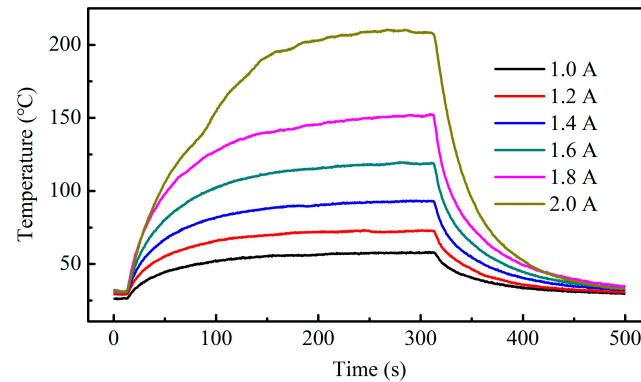
A programmable DC power supply was used to apply a DC current of 1.8 A to the enameled copper wire. The heating time was set to 100 s, and the variable-stiffness joint was manually controlled to bend at a 120° angle. Then, the heating current was turned off, and the variable-stiffness joint's shape was allowed to lock (at this time, the temperature dropped below 50 °C). Similarly, after heating for 100 s, the variable-stiffness joint was manually controlled to return it to its original state. Then, the heating current was turned off again, and the shape was allowed to lock. This sequence of steps was repeated 50 times to complete the cyclic deformation ability test.

### 3. Stiffness Control of the Variable-Stiffness Joints

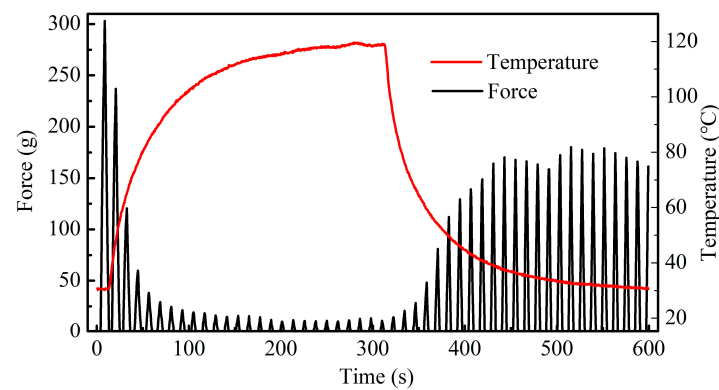
First, we analyzed the heating curves of the variable-stiffness joint under different heating currents. A programmable DC power supply was used to apply a heating current to both ends of the enameled copper wire during testing. K-type thermocouples were used to measure the temperature of the target heating location in the specimen, and data acquisition cards were used to collect the data. As the heating current increased, the temperature at which the variable-stiffness joint reached a stable state increased (Figure 3). At a heating current of 2.0 A, the temperature corresponding to the stable state reached 210 °C, which would cause the PLA structure to melt. However, if the heating current were extremely low, it would be difficult for PLA to undergo the phase transition. Therefore, to determine a reasonable heating current, we simultaneously obtained the temperature curve of the variable-stiffness joint and the deformation force curve under cyclic bending. During the test, we installed a variable-stiffness joint on a self-designed bending testing machine. K-type thermocouples were used to obtain the temperature data during the cyclic bending experiments, and the movement speed of the fixture was 50 mm/min. The test results are presented in Figure 4. As the temperature increased, the bending force of the PLA structure decreased gradually, and after 200 s, the bending force gradually approached zero. After the heating current was turned off, the bending force gradually recovered as the temperature decreased.

For a more effective analysis, we calculated the bending modulus of the PLA structure at different temperatures based on Figure 4 and Section 2.3. The results are shown in Figure 5. Based on the calculation results, the bending modulus of the sample gradually decreased as the temperature increased. At 100 °C, the bending modulus decreased from 3.21 GPa at room temperature to 0.33 GPa, corresponding to 10.2% of the original value. The analysis suggested that owing to the presence of silicone at the joint, a certain degree of stiffness was maintained after heating. In addition, the designed clamp had gaps owing to the need to measure the cyclic bending force during the test. Therefore,

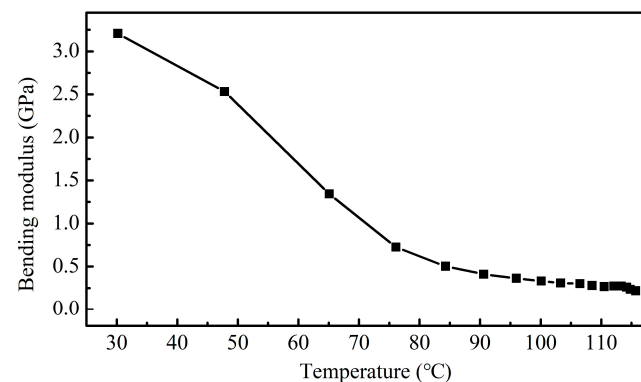
the small deformation of the PLA structure after cooling and hardening decreased the actual displacement loading during the measurements, resulting in the measured force not returning to its initial state after cooling (Figure 4). After adjusting the starting point of the displacement loading, we subjected the specimens to tests at room temperature again, and the results showed that their bending moduli were completely restored.



**Figure 3.** Heating curves of the variable-stiffness joint.



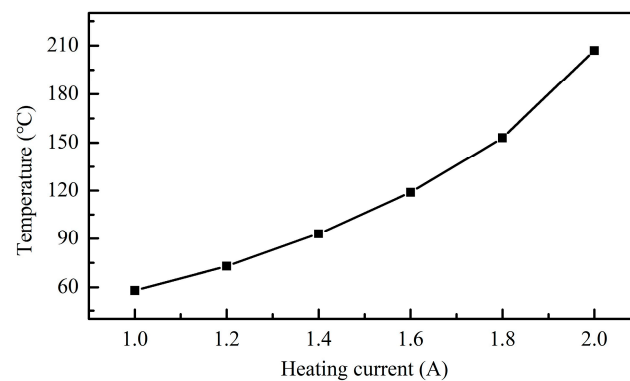
**Figure 4.** Heating curves and deformation force under cyclic bending of the variable-stiffness joint, at a heating current of 1.6 A.



**Figure 5.** Bending modulus of the variable-stiffness joint as a function of the heating temperature.

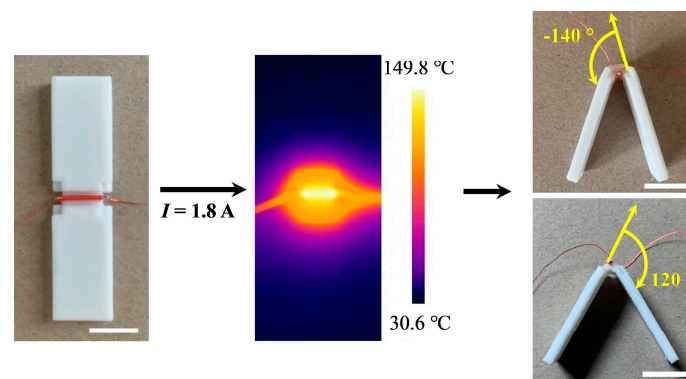
Figure 6 shows the relationship between heating current and stable heating temperature. It can be seen that when the heating current was 1.4 A, the stable heating temperature was 93 °C, and the variable-stiffness joint could not be heated to an effective deformation temperature (100 °C). When the heating current was 2.0 A, the stable heating temperature was 207 °C, which caused the PLA structure to melt. In addition, as shown in Figure 3, a heating current of 1.8 A could increase the temperature of the variable-stiffness joint from room temperature to 100 °C within 40 s. The stable heating temperature at a heating

current of 1.8 A was about 150 °C. After turning off the heating current, the time required for the variable-stiffness joint temperature to drop to 50 °C (at this time, the stiffness was sufficiently restored, as shown in Figure 3) was about 84 s. Therefore, the time required for the variable-stiffness joint to achieve shape control at a heating current of 1.8 A was approximately 124 s. When the heating current was 1.6 A, it took 82 s to raise the temperature of the variable-stiffness joint from room temperature to 100 °C; after turning off the heating current, the time required to reduce the steady-state heating temperature from 119 °C to 50 °C was approximately 67 s. The time required for the variable-stiffness joint to achieve shape control at a heating current of 1.6 A was approximately 149 s. In addition, the heating temperature, from room temperature to 150 °C, was within the temperature range of use of the silicone glue. To summarize, we selected a heating current of 1.8 A for the variable-stiffness joint.

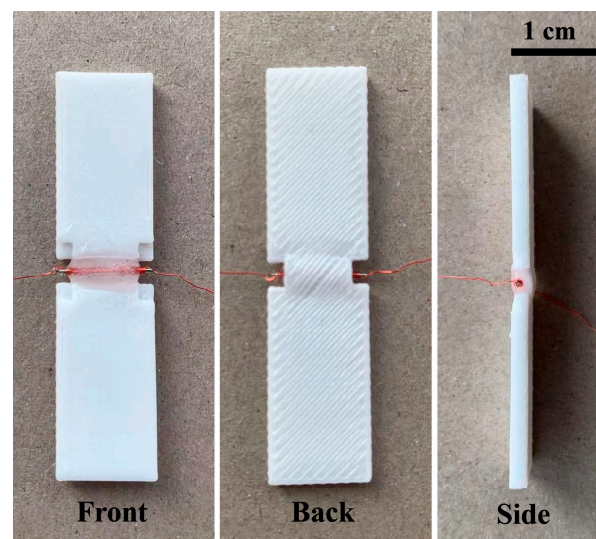


**Figure 6.** Relationship between heating current and stable heating temperature.

We also tested the deformability of the variable-stiffness joint, and the results are shown in Figure 7. The stable heating temperature for a heating current of 1.8 A was 149.8 °C. After reaching a softened state, the variable-stiffness joint be manually bent, and the bending angle ranged between  $-140^{\circ}$  and  $120^{\circ}$ . In addition, we conducted cyclic deformation experiments to test the reusability of the variable-stiffness joint; the specific experimental method can be found in Section 2.4. Figure 8 shows a variable stiffness joint that completed 50 cyclic deformation tests. The back of the variable stiffness joint was not smooth enough, but it still maintained its original structural strength and toughness (Movie S1). In addition, the silicone glue did not show signs of aging and peeling. Based on the degree of tightening of the variable stiffness joint after each experiment, we concluded that it could still achieve deformation control after more than 50 deformation cycles.



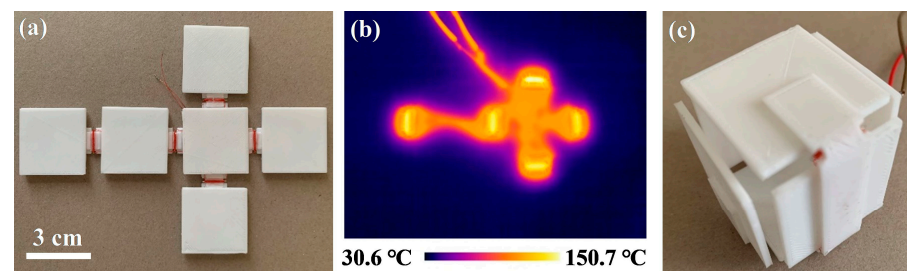
**Figure 7.** Bending capacity of the variable-stiffness joint (scale bar = 2 cm). The stable heating temperature for a 1.8 A heating current was 149.8 °C; at this temperature, the variable-stiffness joint could be manually bent after reaching a softened state. The bending angle ranged between  $-140^{\circ}$  and  $120^{\circ}$ .



**Figure 8.** Variable-stiffness joint after 50 cycles of deformation.

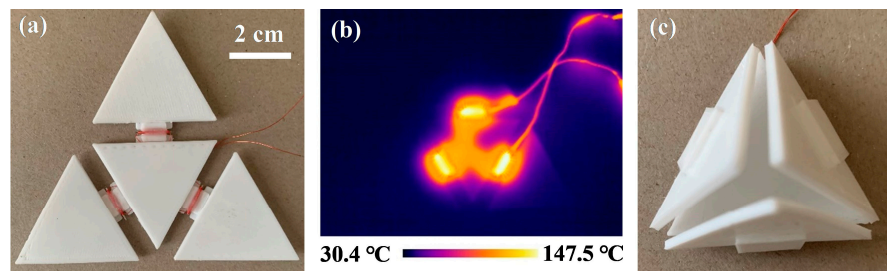
#### 4. Programmable Structure Based on Variable-Stiffness Joints

In this section, three types of variable-stiffness structures are presented. Figure 9a shows a hexahedral unfolded structure that comprises six square structures and one cross-shaped skeleton, which were PLA structures prepared using FDM 3D printing. The cross-shaped skeleton had five variable-stiffness joints, and the enameled copper wires of each variable-stiffness joint were connected in series. We applied a heating current of 1.8 A to both ends of the enameled copper wire. The heating temperature on each variable-stiffness joint was 150.7 °C, reaching the deformation temperature (Figure 9b). Next, we manually bent each variable-stiffness joint at 90° and obtained a hexahedral structure after cooling (Figure 9c).



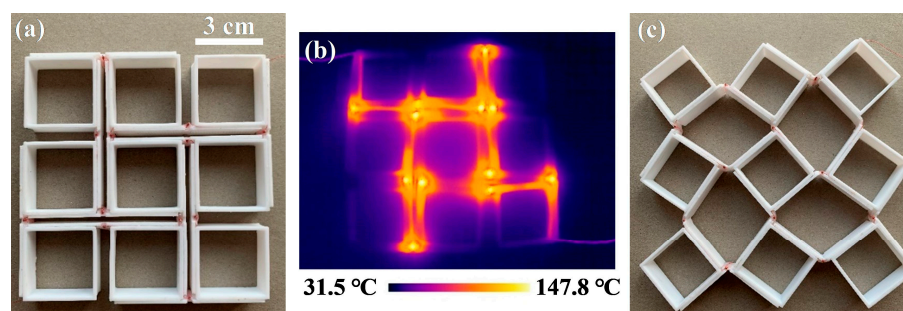
**Figure 9.** Deformable hexahedral box. (a) Initial shape; (b) thermal imaging of the sample reaching a stable temperature under a current of 1.8 A; (c) reconstructed shape.

Figure 10a shows a tetrahedral unfolding structure that comprises a four-triangle structure and a three-pronged star skeleton, which were the PLA structures prepared using the FDM 3D printing process. The skeleton contained three variable-stiffness joints, and the enameled copper wires of each variable-stiffness joint were connected in series. The triangular structure was bonded to the skeleton using silicone glue. We applied a heating current of 1.8 A to both ends of the enameled wire. The stable heating temperature on each variable-stiffness joint was 147.5 °C (Figure 10b), reaching the deformation temperature. After cooling, we manually bent each variable-stiffness joint to obtain a tetrahedral structure, as shown in Figure 10c.



**Figure 10.** Deformable tetrahedral box. (a) Initial shape; (b) thermal imaging of the sample reaching a stable temperature under a current of 1.8 A; (c) reconstructed shape.

We constructed a  $3 \times 3$ -array deformable structure composed of boxes and consisting of twelve variable-stiffness joints, as shown in Figure 11a. Silicone glue was used to bond each box unit to the variable-stiffness joints, and the enameled copper wires were connected in series. We applied a heating current of 1.8 A to both ends of the enameled wire. The temperature of each variable-stiffness joint was  $147.8 \text{ }^\circ\text{C}$  (Figure 11b), and the deformation temperature was reached. Finally, we manually stretched the  $3 \times 3$ -array structure to the shape shown in Figure 11c.

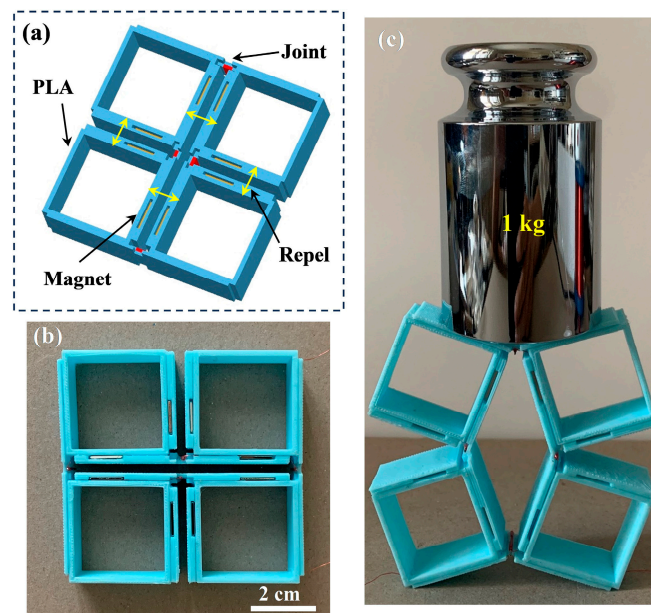


**Figure 11.** Image of the  $3 \times 3$ -box array variable-stiffness structure. (a) Initial shape; (b) thermal imaging of the sample reaching a stable temperature under a heating current of 1.8 A; (c) reconstructed shape.

### 5. Self-Deforming Actuators Based on Variable-Stiffness Joints

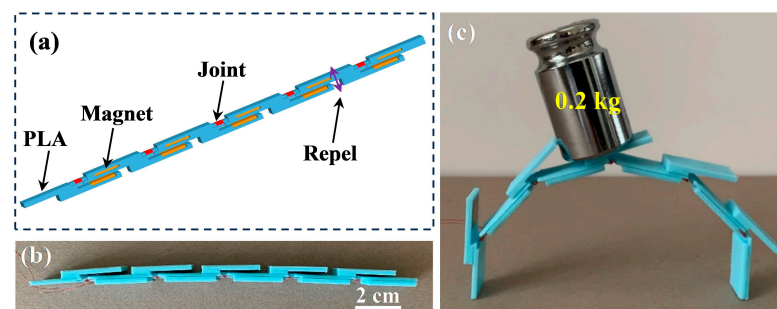
In most applications, variable-stiffness structures must be able to deform autonomously. Therefore, we propose a self-deformable variable-stiffness structure based on a magnetic drive to obtain variable-stiffness actuators that can be expanded and deployed.

Figure 12a shows a  $2 \times 2$ -array variable-stiffness structure composed of boxes. The box units were connected using variable-stiffness joints. Two adjacent box units were arranged with square magnets near the variable-stiffness joint, and the magnetic poles between the two magnets were opposite, that is, they exerted repulsive forces. When the variable-stiffness joint was not heated and softened, it maintained a high stiffness; thus, the repulsive force between the magnets did not deform the structure. When the stiffness of the variable-stiffness joint decreased after applying a heating current, the structure could automatically deform under the repulsive force between the magnets. Figure 12b shows the prepared  $2 \times 2$ -box array structure with self-deforming ability. The magnet was a NdFeB permanent magnet with dimensions of  $1 \text{ cm} \times 1 \text{ cm} \times 0.1 \text{ cm}$ . A heating current of 1.8 A was applied to the enameled wire. With an increase in the heating temperature, the structure deformed under the repulsive force of the magnet. The heating current was turned off, and the variable-stiffness joint was allowed to cool to obtain the shape shown in Figure 8c. After deformation, the  $2 \times 2$ -box array structure could carry objects weighing more than 1 kg (Figure 12c), indicating a satisfactory load capacity.



**Figure 12.** Image of the  $2 \times 2$ -box array variable-stiffness structure with self-deforming ability. (a) Diagram of the structure; (b) photograph of the structure; (c) load-bearing capacity after deformation.

Figure 13a shows a variable-stiffness structure in the shape of a long strip. Five variable-stiffness joints were arranged on the elongated structure, with a pair of magnets positioned at the front end of each variable-stiffness joint. Similarly, the magnetic poles of two magnets were placed so that they exerted repulsive forces. When a variable-stiffness joint was heated, the structure could automatically bend under the repulsive force of the magnet. Figure 13b shows a variable-stiffness long strip capable of undergoing self-deformation. Its magnet material and size were consistent with those of the  $2 \times 2$ -box array variable-stiffness structure previously described. The structure became semicircular after heating and cooling and could resist loads exceeding 0.2 kg, as shown in Figure 13c.



**Figure 13.** Variable-stiffness long strip with self-deforming ability. (a) Diagram of the structure; (b) photograph of the structure; (c) load-bearing capacity after deformation.

## 6. Electromagnetically Driven Mechanical Gripper Based on Variable-Stiffness Joints

Although the above-described self-deforming actuators do not require an external drive, they can only perform a single task and cannot achieve reverse drive or cyclic drive, which greatly limits their application. In this section, we describe a variable-stiffness actuator that integrates an electromagnetic coil and a magnet; specifically, it is an electromagnetically driven mechanical gripper, as shown in Figure 14. The electromagnetically driven mechanical gripper consisted of a PLA support structure, a PLA three-finger gripper, variable-stiffness joints, magnets, and coils. The three-finger gripper was fixed to the support structure, with three variable-stiffness joints located at the roots of the three fingers, and a magnet located at the outer end of the variable-stiffness joints. The three coils

were fixed to the support structure at the level of the magnets. The purpose of the three magnets in the mechanical gripper was to provide a stable magnetic field. When direct current was applied to the coils, a magnetic field with the same or opposite direction to those of the magnets was formed, and the electromagnetic force generated between the coils and the magnets drove the mechanical gripper to close or open. In addition, each gripper was bonded to a polydimethylsiloxane (PDMS) layer to improve the frictional force when grasping an object. The support structure and mechanical gripper were prepared using the FDM 3D printing process. The enameled wires of each variable-stiffness joint were connected in series, and the coil was customized for processing. The magnet was a NdFeB permanent magnet with dimensions of  $1\text{ cm} \times 1\text{ cm} \times 0.2\text{ cm}$ . Silicone glue and screws were used to fix the parts of the structure.

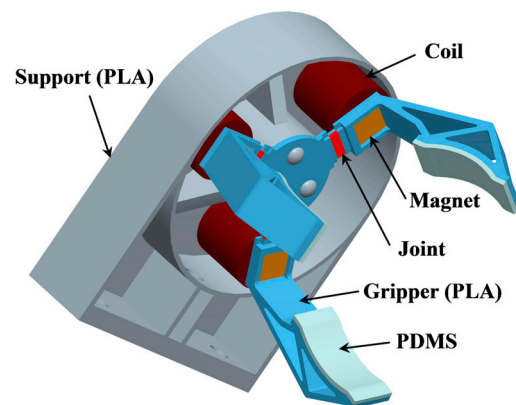


**Figure 14.** Diagram of the electromagnetically driven mechanical gripper.

Figure 15a shows the deformation state of the electromagnetically driven mechanical gripper under different driving currents. Figure 15b shows the relationship between the deformation angle  $\theta$  of the fingers and the driving current. The deformation angle  $\theta$  increased with the increase in driving current, and their relationship was linear. When the driving current was 1.1 A, the fingertips were in contact with each other, and the gripper reached the maximum deformation angle. However, the linear curve showing the relationship between the deformation angle  $\theta$  of the fingers and the driving current does not start from the origin. This is because the mechanical gripper was positioned downward, and even when the drive current was not applied onto the coils, the fingers underwent a slight deformation under gravity.

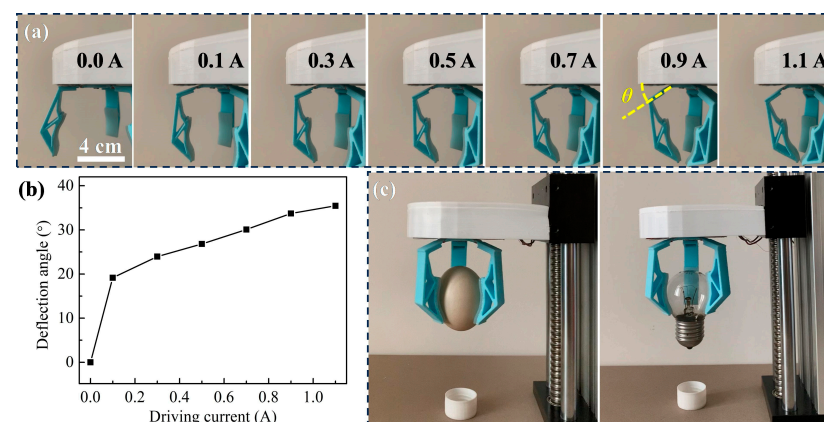


**Figure 15.** Basic performance of the electromagnetically driven mechanical gripper, at a heating current of 1.8 A. (a) Deformation state under different driving currents; (b) relationship between driving current and deflection angle of the mechanical gripper; (c) clamping of an egg and a light bulb.

The operation process of this mechanical gripper was as follows: (a) A heating current was applied to the enameled copper wire to control the softening of the gripper fingers. (b) A driving current was applied to the three coils such that their magnetic field direction was opposite to the magnetic field direction of the magnets, driving the three-finger gripper to close and grip the object. (c) The heating current applied to the enameled copper wire was turned off, and the temperature of the variable-stiffness joints was allowed to decrease to room temperature. (d) The driving current applied to the coils was turned off, and the stiffness of the variable-stiffness joints returned to the initial values, thus enabling a stable clamping of the object. The mechanical gripper stably held an egg and a light bulb (Figure 15c). In addition, through the above process, the gripper could also release the grasped object, as shown in Supplementary Video S1.

The advantages of the electromagnetically driven mechanical gripper are as follows: (1) It achieves variable-stiffness control, which can effectively decrease the driving energy in applications where objects are held for an extended period. (2) By utilizing a small electromagnetic force to control the deformation, it can adapt to the external dimensions of the object being held without generating excessive pressure. In addition, it utilizes the variable-stiffness shape-locking ability to grip fragile items. (3) By using variable-stiffness joints and the 3D printing technology, mechanical grippers can be rapidly designed and manufactured.

## 7. Conclusions

In this study, we developed a variable-stiffness joint consisting of steel needles wrapped with an enameled wire arranged in the grooves of a PLA structure and bonded with silicone glue. Stiffness control was achieved by applying a current to the enameled wire to induce a phase transition in the PLA grooves. The steel needles served as the rotation axis to prevent torsional deformation after joint softening. Research showed that when the heating temperature of a variable-stiffness joint is 100 °C, the bending modulus continuously decreases from 3.21 GPa at room temperature to 0.33 GPa. The purpose of stiffness control was achieved, with a bending angle ranging between  $-140^\circ$  and  $120^\circ$ . We found that to achieve a good operational temperature and prevent the melting of the PLA structure due to an excessive temperature, the heating current had to be 1.8 A, with a stable heating temperature of approximately 150 °C.

Variable-stiffness joints were used to design a hexahedral variable-stiffness structure, a tetrahedral variable-stiffness structure, and  $3 \times 3$ -box array variable-stiffness structure. These structures effectively demonstrated the excellent deformation ability of variable-stiffness structures based on variable-stiffness joints. A design scheme was developed for a variable-stiffness actuator that can autonomously deform based on a magnetic drive, achieving the expansion and deployment functions of the structure. This actuator could be used as an antenna and solar panel deployment structure for small spacecraft or in the medical field as an orthopedic support to replace gypsum and may be combined with an external magnetic field control to enter narrow spaces for field rescue tasks. It is hoped that these potential applications can be realized in the near future with further research. We also designed an electromagnetically driven mechanical gripper based on variable-stiffness joints, effectively decreasing the driving energy in applications where objects are held for extended periods using variable-stiffness control.

**Supplementary Materials:** The following supporting information can be downloaded at: <https://www.mdpi.com/article/10.3390/act12110397/s1>, Video S1: The operation process of this mechanical gripper.

**Author Contributions:** Conceptualization, Q.W. and C.G.; Data curation, Q.W. and X.L.; Formal analysis, Q.W.; Methodology, X.L. and P.J.; Validation, X.L.; Visualization, Q.W.; Writing—original draft, Q.W., C.G. and Y.S.; Writing—review and editing, Q.W., X.L., P.J., C.G. and Y.S. All authors have read and agreed to the published version of the manuscript.

**Funding:** This research was funded by the Natural Science Foundation of Jiangsu Province, grant BK20200984.

**Data Availability Statement:** Not applicable.

**Conflicts of Interest:** The authors declare no conflict of interest.

## References

1. Aksoy, B.; Shea, H. Multistable shape programming of variable-stiffness electromagnetic devices. *Sci. Adv.* **2022**, *8*, eabk0543. [[CrossRef](#)] [[PubMed](#)]
2. Wang, L.Y.; Yang, Y.; Chen, Y.H.; Majidi, C.; Iida, F.; Askounis, E.; Pei, Q.B. Controllable and reversible tuning of material rigidity for robot applications. *Mater. Today* **2018**, *21*, 563–576. [[CrossRef](#)]
3. Baines, R.L.; Booth, J.W.; Fish, F.E.; Kramer-Bottiglio, R. Toward a bio-inspired variable-stiffness morphing limb for amphibious robot locomotion. In Proceedings of the 2nd IEEE International Conference on Soft Robotics (RoboSoft), Seoul, Republic of Korea, 14–18 April 2019.
4. Meerbeek, I.M.V.; Murray, B.C.M.; Kim, J.W.; Robinson, S.S.; Zou, P.X.; Silberstein, M.N.; Shepherd, R.F. Morphing metal and elastomer bicontinuous foams for reversible stiffness, shape memory, and self-healing soft machines. *Adv. Mater.* **2016**, *28*, 2801–2806. [[CrossRef](#)] [[PubMed](#)]
5. Al-Rubaiai, M.; Pinto, T.; Qian, C.Q.; Tan, X.B. Soft actuators with stiffness and shape modulation using 3D-printed conductive polylactic acid material. *Soft. Robot.* **2019**, *6*, 318–322. [[CrossRef](#)] [[PubMed](#)]
6. Buckner, T.L.; Bilodeau, R.A.; Kim, S.Y.; Kramer-Bottiglio, R. Roboticizing fabric by integrating functional fibers. *Proc. Natl. Acad. Sci. USA* **2020**, *117*, 25360–25369. [[CrossRef](#)] [[PubMed](#)]
7. Baines, R.; Patiballa, S.K.; Booth, J.; Ramirez, L.; Sipple, T.; Garcia, A.; Fish, F.; Kramer-Bottiglio, R. Multi-environment robotic transitions through adaptive morphogenesis. *Nature* **2022**, *610*, 283–289. [[CrossRef](#)] [[PubMed](#)]
8. Wang, Q.; Li, L.Z.; Lu, X.L.; Dong, X.; Jiang, P.; Pan, H.J.; Liu, Y.; Yuan, N.Y.; Ding, J.N. Programmable design and fabrication of 3D variable-stiffness structure based on patterned graphene-heating network. *Adv. Intell. Syst.* **2023**, *5*, 2300032. [[CrossRef](#)]
9. Zhai, Z.; Wang, Y.; Jiang, H. Origami-inspired, on-demand deployable and collapsible mechanical metamaterials with tunable stiffness. *Proc. Natl. Acad. Sci. USA* **2018**, *115*, 2032–2037. [[CrossRef](#)]
10. Hwang, D.; Barron, E.J.; Haque, A.B.M.T.; Bartlett, M.D. Shape morphing mechanical metamaterials through reversible plasticity. *Sci. Robot.* **2022**, *7*, eabg2171. [[CrossRef](#)]
11. Yang, Y.; Chen, Y.; Li, Y.; Wang, Z.; Li, Y. Novel variable-stiffness robotic fingers with built-in position feedback. *Soft. Robot.* **2017**, *4*, 338–352. [[CrossRef](#)]
12. Bilodeau, R.A.; Yuen, M.C.; Kramer-Bottiglio, R. Addressable, stretchable heating silicone sheets. *Adv. Mater. Technol.* **2019**, *4*, 1900276. [[CrossRef](#)]
13. Thien, P.; Le, Q.N.; Luong, Q.V.; Kim, H.H.; Park, H.M.; Kim, Y.J. Tendon-driven gripper with variable stiffness joint and water-cooled SMA springs. *Actuators* **2023**, *12*, 160.
14. Yang, Y.; Chen, Y.H.; Li, Y.T.; Chen, M.Z.Q.; Wei, Y. Bioinspired robotic fingers based on pneumatic actuator and 3D printing of smart material. *Soft. Robot.* **2017**, *4*, 147–162. [[CrossRef](#)] [[PubMed](#)]
15. Zhang, Y.; Zhang, N.; Hingorani, H.; Ding, N.; Wang, D.; Yuan, H.; Zhang, B.; Gu, G.; Ge, Q. Fast-response, stiffness-tunable soft actuator by hybrid multimaterial 3D printing. *Adv. Funct. Mater.* **2019**, *29*, 1806698. [[CrossRef](#)]
16. Wang, W.; Yu, C.Y.; Serrano, P.A.A.; Ahn, S. Shape memory alloy-based soft finger with changeable bending length using targeted variable stiffness. *Soft. Robot.* **2019**, *7*, 283–291. [[CrossRef](#)] [[PubMed](#)]
17. Song, E.J.; Lee, J.S.; Moon, H.; Choi, H.R.; Koo, J.C. A multi-curvature, variable stiffness soft gripper for enhanced grasping operations. *Actuators* **2021**, *10*, 316. [[CrossRef](#)]
18. Piskarev, E.; Shintake, J.; Ramachandran, V.; Baugh, N.; Dickey, M.D.; Floreano, D. Lighter and stronger: Cofabricated electrodes and variable stiffness elements in dielectric actuators. *Adv. Intell. Syst.* **2020**, *2*, 2000069. [[CrossRef](#)]
19. Jiang, P.; Yang, Y.; Chen, M.Z.Q.; Chen, Y. A variable stiffness gripper based on differential drive particle jamming. *Bioinspir. Biomim.* **2019**, *14*, 036009. [[CrossRef](#)] [[PubMed](#)]
20. Wang, W.; Ahn, S. Shape memory alloy-based soft gripper with variable stiffness for compliant and effective grasping. *Soft. Robot.* **2017**, *4*, 379–389. [[CrossRef](#)] [[PubMed](#)]
21. Zhou, J.; Chen, Y.; Hu, Y.; Wang, Z.; Li, Y.; Gu, G.; Liu, Y. Adaptive variable stiffness particle phalange for robust and durable robotic grasping. *Soft. Robot.* **2020**, *7*, 743–757. [[CrossRef](#)]
22. Lussi, J.; Mattmann, M.; Sevim, S.; Grigis, F.; Marco, C.D.; Chautems, C.; Pané, S.; Puigmartí-Luis, J.; Boehler, Q.; Nelson, B.J. A submillimeter continuous variable stiffness catheter for compliance control. *Adv. Sci.* **2021**, *8*, e2101290. [[CrossRef](#)] [[PubMed](#)]
23. Shah, D.S.; Yang, E.J.; Yuen, M.C.; Huang, E.C.; Kramer-Bottiglio, R. Jamming skins that control system rigidity from the surface. *Adv. Funct. Mater.* **2020**, *31*, 2006915. [[CrossRef](#)]
24. Piskarev, Y.; Shintake, J.; Chautems, C.; Lussi, J.; Boehler, Q.; Nelson, B.J.; Floreano, D. A variable stiffness magnetic catheter made of a conductive phase-change polymer for minimally invasive surgery. *Adv. Funct. Mater.* **2022**, *32*, 2107662. [[CrossRef](#)]
25. Giachini, P.A.G.S.; Gupta, S.S.; Wang, W.; Wood, D.; Yunusa, M.; Baharlou, E.; Sitti, M.; Menges, A. Additive manufacturing of cellulose-based materials with continuous, multidirectional stiffness gradients. *Sci. Adv.* **2020**, *6*, eaay0929. [[CrossRef](#)] [[PubMed](#)]
26. Shin, S.; So, H. Time-dependent motion of 3D-printed soft thermal actuators for switch application in electric circuits. *Addit. Manuf.* **2021**, *39*, 101893. [[CrossRef](#)]

27. Travieso-Rodriguez, J.A.; Jerez-Mesa, R.; Llumà, J.; Traver-Ramos, O.; Gomez-Gras, G.; Rovira, J.J.R. Mechanical properties of 3D-printing polylactic acid parts subjected to bending stress and fatigue testing. *Materials* **2019**, *12*, 3859. [[CrossRef](#)] [[PubMed](#)]
28. Yuen, M.C.; Bilodeau, R.A.; Kramer, R.K. Active variable stiffness fibers for multifunctional robotic fabrics. *IEEE Robot. Autom. Let.* **2016**, *1*, 708–715. [[CrossRef](#)]
29. Zheng, W.; Wei, K.; Zhu, S.; Wang, J.; Niu, F.; Liu, G.; Yang, R. Multi-function untethered actuator based on Ni-Ti alloy and polylactic acid. *Sensor. Actuat. A phys.* **2022**, *344*, 113697. [[CrossRef](#)]
30. Park, J.; Lee, H.; Kee, H.; Park, S. Magnetically steerable manipulator with variable stiffness using graphene polylactic acid for minimally invasive surgery. *Sensor. Actuat. A phys.* **2020**, *309*, 112032. [[CrossRef](#)]

**Disclaimer/Publisher's Note:** The statements, opinions and data contained in all publications are solely those of the individual author(s) and contributor(s) and not of MDPI and/or the editor(s). MDPI and/or the editor(s) disclaim responsibility for any injury to people or property resulting from any ideas, methods, instructions or products referred to in the content.